frontiers | Frontiers in Earth Science

ORIGINAL RESEARCH
published: 14 June 2022
doi: 10.3389/feart.2022.925636

Effects of Rainfall on Mechanical Behaviors of Residual-Soil Landslide

Yong He[1,2,3], *Zhi-Peng Yu*[1,2], *Zhao Zhang*[1,2,3]*, *Bin Chen*[4] and *Ke-Neng Zhang*[1,2]

[1]Key Laboratory of Metallogenic Prediction of Nonferrous Metals and Geological Environment Monitoring (Central South University), Ministry of Education, Changsha, China, [2]School of Geosciences and Info-Physics, Central South University, Changsha, China, [3]Key Laboratory of Geotechnical and Underground Engineering of Ministry of Education and Department of Geotechnical Engineering, Tongji University, Shanghai, China, [4]Hunan Provincial Key Laboratory of Geomechanics and Engineering Safety, Xiangtan University, Xiangtan, China

Rainfall-induced landslides commonly occur in residual-soil layers of Chenzhou city, China. Slope failure induced by rainfall is intimately related to changes in the mechanical property and microstructures of residual soils. In this study, series of direct shear tests were respectively conducted on four typical residual soils from the area of Chenzhou to study influences of rainwater on their mechanical behaviors. Meanwhile, X-ray diffraction (XRD) tests and scanning electron microscope (SEM) tests were also performed to investigate microstructure characteristic of several types of soils. Experimental results revealed that the shear strength of soils decreased with increasing water content and its development trends were obviously influenced by the types of residual soils. Meanwhile, the shear strength of soils increased with the increase of vertical loads, and the relationship between them could be well expressed by a linear function. As water content increased, the calculated cohesions and internal friction angles both decreased. XRD observations implied that several residual soils showed rich clay minerals, including pyrophyllite, illite, kaolinite and montmorillonite, etc. Microstructures of these soils presented a sheet-structure system which was composed of various-sized clay particles. During hydration, these clay minerals gradually transferred from a face-face arrangement to face-edge or even edge-edge one, leading to the softening of clay particles and the reduction of the contact force between soil particles.

Keywords: landslide, shear strength, residual soil, microstructure, mechanical behavior

OPEN ACCESS

Edited by:
Irasema Alcántara-Ayala, National Autonomous University of Mexico, Mexico

Reviewed by:
Luqi Wang, Chongqing University, China
Bing Bai, Beijing Jiaotong University, China

***Correspondence:**
Zhao Zhang
zhangzhaozn@163.com

Specialty section:
This article was submitted to Geohazards and Georisks, a section of the journal Frontiers in Earth Science

Received: *21 April 2022*
Accepted: *30 May 2022*
Published: *14 June 2022*

Citation:
He Y, Yu Z-P, Zhang Z, Chen B and Zhang K-N (2022) Effects of Rainfall on Mechanical Behaviors of Residual-Soil Landslide. Front. Earth Sci. 10:925636. doi: 10.3389/feart.2022.925636

1 INTRODUCTION

China is a country with frequent landslide activities. Landslide will seriously threaten the safety of human life and property, e.g., Sugarwumei landslide in 2018, Shuicheng landslide in 2019 and Manisales landslide in 2019, etc. The occurrence of landslides is normally related to mechanical properties of sliding-surface soils, especially for the soil layers with poor properties (Zhang et al., 2016; Xiao et al., 2021; Yin et al., 2022). Large number of studies demonstrated that landslides commonly happen in rainy seasons because the rainfall causes the deterioration in the mechanical property of slope soils. Wen et al. (2019) studied the triggering mechanism of rainfall on slow-dip red-bed rock landslide and concluded that the formation process of landslides could be closely classified into four stages: 1) the fracture development stage resulted from the rainfall infiltration; 2) the shear-strength decreasing stage in the weak zone; 3) the rising stage of the pore water pressure and uplift pressure; and 4) the instability and sliding process of slopes. Zhu et al. (2019) conducted

laboratory model tests on the loess-mudstone slope under two heavy rainfall patterns, and results revealed that the slope instability both occurred on the loess-mudstone contact surface. The creeping-fracturing instability happened under a continuous strong rainfall, while a sliding-fracturing instability occurred in an intermittent strong rainfall, which depended on the infiltration rates of rainwater. Moreover, Miščević and Vlastelica (2014) investigated the influences of weathering on the stability of soft-rock slope and pointed out that the instability modes of marl slope were primarily controlled by a weak surface generated during the weathering process. Khan et al. (2017) explored the failure mechanism of the shallow expansive soil slope. Experimental results demonstrated that as rainwater infiltrated along the surface cracks, shear strength of the soils in the sliding zone obviously decreased, which was the main reason of landslides. Therefore, it is necessary to study the mechanical behavior of sliding-zone soils and its sensitivity to water changes for assessment of the slope stability.

It is well recognized that the rainfall infiltration can cause a dissipation of the soil suction and a reduction of the shear strength when the unsaturated soil slopes are subjected to rainfall (De Vita et al., 1998; Patuti et al., 2017). Farooq et al. (2004) and Orense et al. (2004) pointed out that the pore pressure inside slope soil gradually increased from a negative value to a higher one with the infiltration of rainwater, and the effective stress accordingly decreased until the failure occurred. The strength of soil actually originates from frictional resistance and bonding force between soil particles, which are associated with fabric changes. Studies demonstrated that the shear strength of unsaturated soils normally decreased with increasing water content, and its reduction was intimately related to the soil property, e.g., microstructure, mineral composition, the stress history and the original fabric (Fredlund et al., 1996; He et al., 2020, 2021; Zhang et al., 2021). For unsaturated sandy soils, the capillary force between soil particles reduces and the cohesion generated by the capillary water decreases during the infiltration of rainwater. Meanwhile, small sand particles are likely to transport through large inter-particle pores under high groundwater pressure (Bai et al., 2021a; 2021b). While for unsaturated clayey soils, the interaction between clay particles was controlled by the absorptive force of absorbed water and the capillary force of capillary water. The shear strength of soil was dominated by the absorptive force in low water contents (or high suctions), while in high water contents (or low suctions), the change of shear strength was primarily influenced by the capillary water (Mitchell and Soga, 2005; Lu, 2016). Therefore, the rainfall-induced strength changes for clayey soil appear to be more complicate due to complex mineral composition and fabric changes.

In this study, several typical residual soils were extracted from the landslide zones in Chenzhou, Hunan province. Series of shear tests, X-ray diffraction (XRD) tests and scanning electron microscope (SEM) tests were carried out to investigate mechanical property and microstructures of several soils at varied water contents, respectively. The changes of strength parameters (e.g., shear strength, cohesion and internal friction angle) with water content were analyzed and the corresponding mechanisms were clarified through microstructural observations. These findings provide useful information for deeply understanding the failure mechanism of residual-soil slopes.

2 MATERIALS AND METHODS

2.1 Materials

A western North Pacific Ocean severe tropical storm "Bilis" made landfall on the southeastern coast of mainland China on 14 July 2006. The heavy rainfalls induced by Bilis attacked the Chenzhou city in Hunan province and caused more than 8,000 landslides and mudslides, which killed at least 394 people and left 97 people missing (Ma and Tan, 2009). Field investigation found that most of the landslide sliding zones are in residual soil layers. **Figure 1** presents several typical residual soils widely distributed in this area, including white silty-clay layer (WSC), gray coal-soil layer (GCS) and red-clay layers (RC-I and RC-II). These soil layers are normally considered as the main slip formations of landslides. In this work, four types of residual soils above were selected and remolded. Basic physical properties of these soils are listed in **Table 1**. It can be seen that the natural water contents of four types of soils are all lower than their liquid limits, with a highest water content for the gray coal soil. Two kinds of red clay had high liquid limits and initial void ratios. **Figure 2** shows particle size distribution curves of several soil samples. It can be found that the fine-particles (<0.075 mm) content for all samples is over than 80 %. Red clay sample has the highest clay content, corresponding to a high specific surface area.

The preparation procedure of remodeled samples was carried out with reference to the method proposed by GB/T 50123-2019. The dry density of soil samples was 1.72 ± 0.2 g/cm^3 and the designed moister content range was between 16%–41%.

2.2 Test Instrument and Method

2.2.1 Direct Shear Test

According to the test method (Ministry of Housing and Urban-Rural Development of the People's Republic of China, 2019), a strain-controlled direct shear apparatus was employed for conducting direct shear tests. Four vertical loads (i.e., 100, 200, 300, and 400 kPa) were respectively applied on the soil samples and a shear rate of 0.8 mm/min was adopted for a fast direct shear. Meanwhile, direct shear tests were separately performed on soil samples at various water contents to study effects of water content on shear behavior. There were totally 84 samples for four types of soils in the direct shear test, where 24 for WSC samples, 16 for GCS samples, 20 for RC-I samples and 24 for RC-II samples.

2.2.2 X-Ray Diffraction Measurement

The soil samples were dried at 50°C in oven, finely ground and screened through a 200-mesh sieve to obtain powders for mineralogy characterizations. Characterization by XRD was carried out using the random powder method (Sun et al., 2019). The XRD measurement was carried out by D8 FOCUS (Germany, Bruker) with CuKα radiation (λ = 0.15418 nm) at the ambient temperature of 25°C, operating at 30 mA and 40 kV. The

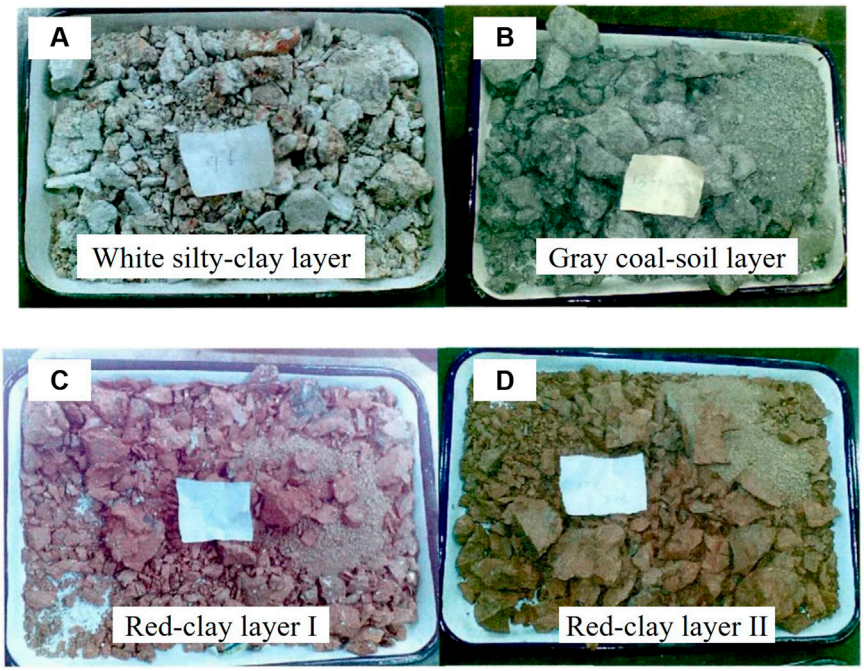

FIGURE 1 | Typical residual soils in Chenzhou area: **(A)** WSC; **(B)** GCS; **(C)** RC-I and **(D)** RC-II.

TABLE 1 | Basic physical properties of typical residual soils.

Number	Sample name	Specific gravity	Water content (%)	Void ratio	Liquid limit (%)	Plastic limit (%)
1	White silty clay	2.69	17.7	0.476	32.3	16.2
2	Gray coal soil	2.72	25.7	0.536	32.9	20.3
3	Red clay I	2.73	20.6	1.098	54.1	19.4
4	Red clay II	2.69	22.4	1.379	49.6	20.2

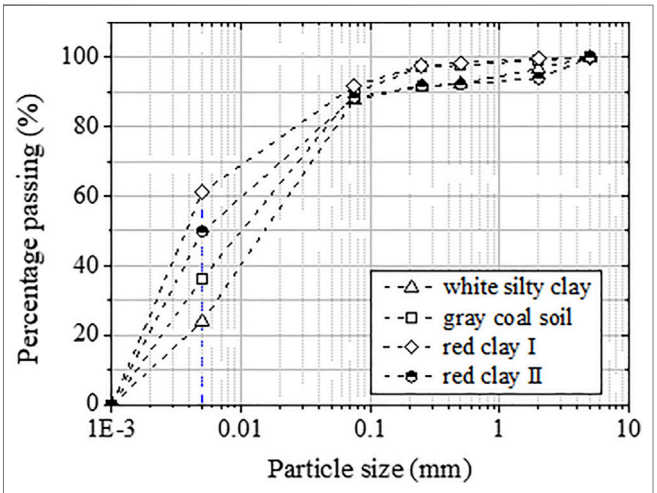

FIGURE 2 | Particle size distribution curves of several residual soils.

measured range was 3°–70° and the 2θ-scanning rate was 2°/min. The JCPDS PDF database was used for the phase identification of the XRD results.

2.2.3 Scanning Electron Microscope Test

To prepare samples of SEM tests, the soil samples were firstly cut into small pieces with dimensions of 10 × 10 × 5 mm (length × width × height) and then rapidly immersed in the previously vacuum-cooled liquid nitrogen. After that, the frozen samples were freeze-dried for 24 h in a vacuumed chamber. SEM tests were performed on the freeze-dried samples using a JSM-6490LV electron microscope scanner.

3 RESULTS AND DISCUSSION

3.1 Shear Property of Residual Soils

Figure 3 shows the changes of shear strength with water content for four soil samples. On the whole, the shear strength of all soil

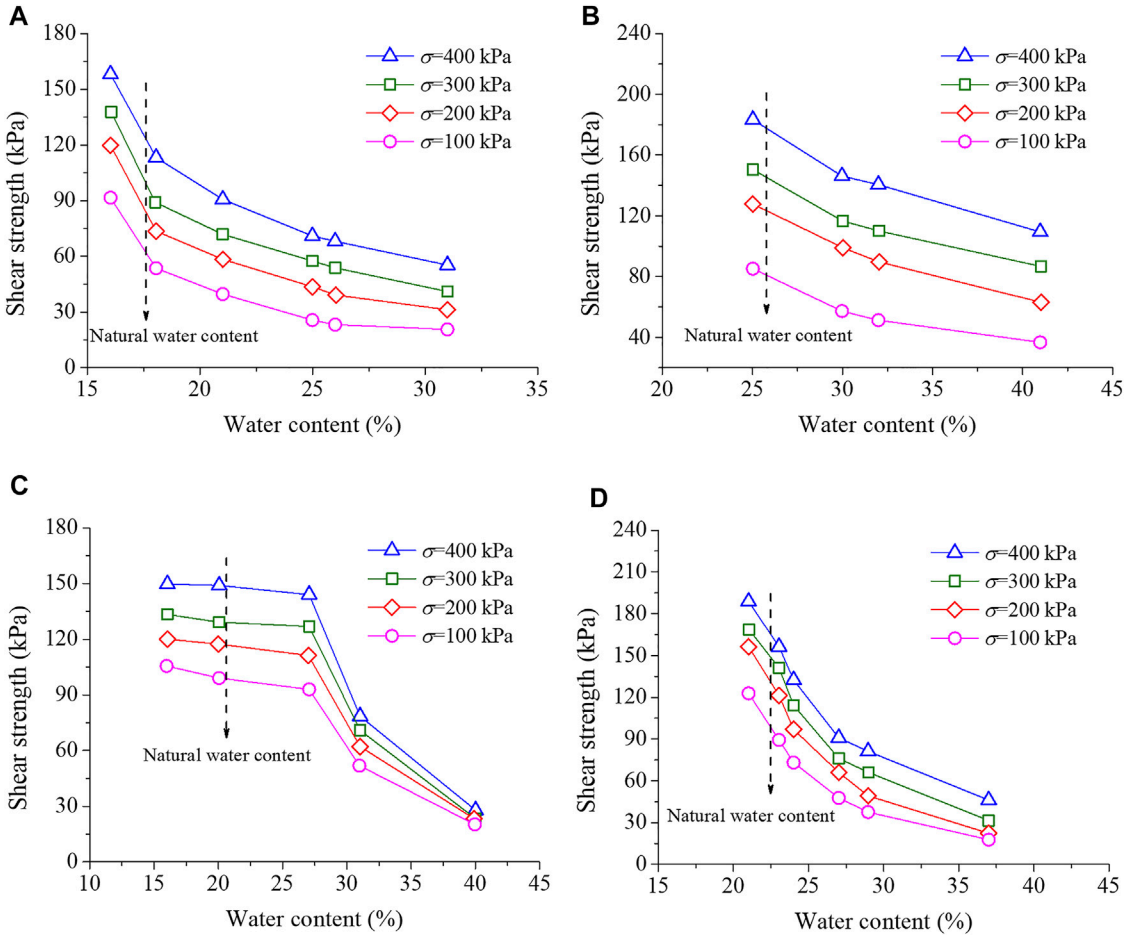

FIGURE 3 | Variations of shear strength with water content for **(A)** WSC samples; **(B)** GCS samples; **(C)** RC-I samples and **(D)** RC-II samples.

samples decreased with increasing water content, but the shear strength for each soil shows different developing trends. For WSC samples, the shear strength firstly decreased quickly with increasing water content and then gradually tended to a stabilization, as shown in **Figure 3A**. At a given water content, the shear strengths of samples increased with the increase of vertical loads. Similar phenomenon was also observed from the curves of gray coal soil (**Figure 3B**). Results in **Figure 3C** demonstrated that the shear strength of RC-I samples slightly reduced as water content increased from 16% to 26%, whereas it obviously decreased with a further increase of water content. Different from RC-I samples, the strength changes for RC-II samples were significant in low water contents, whereas the reducing rate of shear strength became slower in high water contents. According to the natural water contents of several soils, the increases of water content nearby the natural value will cause an obvious reduce of shear strength for WSC, GCS and RC-II samples, excepting for RC-I sample.

Figure 4 presents changes of shear strength with vertical load for soil samples at different water contents. Generally, the relationship between shear strength and vertical load can be described by a linear equation in **Eq. 1**. According to experimental results in **Figure 4**, the fitting curves between shear strength and vertical load could be obtained, and the corresponding parameters ϕ and c are listed in **Table 3**, respectively.

$$\tau_s = \sigma \tan \phi + c \tag{1}$$

where τ_s is the shear strength (kPa) of soil samples; σ is the applied vertical load (kPa) on samples; ϕ is internal friction angle (°) and c is cohesion (kPa). It is noted that for unsaturated soils, the parameters ϕ and c in **Eq. 1** are influenced by the water contents, which is also confirmed from **Table 2**.

Figure 5 shows variations of cohesion c and internal friction angle ϕ with water content, respectively. Results indicated that the c values for WSC, GCS and RC-II samples firstly reduced obviously and then gradually tended to a stable state, but it appeared that the opposite developing trend was observed in RC-I samples. An exponential function (**Eq. 2**) can be tried to describe the relationship between the cohesion and water content, and the corresponding fitting parameters are summarized in **Table 3**. Comparison reveals that this fitting function could give high correlation coefficients (R^2), suggesting a good fitting

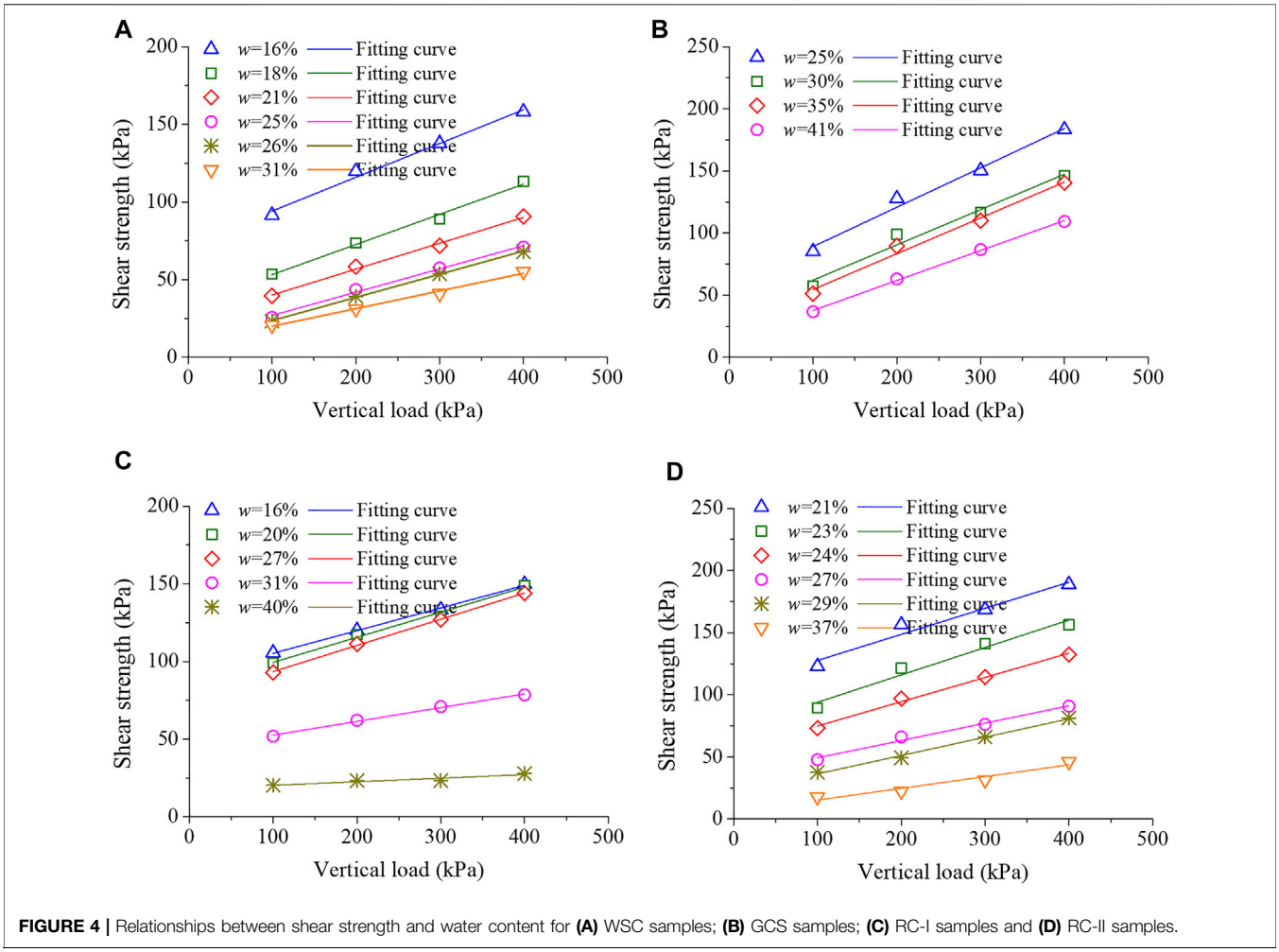

FIGURE 4 | Relationships between shear strength and water content for **(A)** WSC samples; **(B)** GCS samples; **(C)** RC-I samples and **(D)** RC-II samples.

TABLE 2 | Fitting results for relationship between shear strength and vertical load.

Samples	Water content (%)	ϕ	C	R^2	Samples	Water content (%)	ϕ	c	R^2
WSC	16	12.298	72.403	0.986	RC-I	16	8.306	90.710	0.997
	18	10.979	33.786	0.990		20	9.146	83.287	0.987
	21	9.425	23.514	0.994		27	9.592	76.624	0.999
	25	8.531	11.996	0.992		31	5.086	43.693	0.993
	26	8.475	8.707	0.999		40	1.318	17.995	0.824
	31	6.504	8.596	0.989	RC-II	21	11.860	106.600	0.943
GCS	25	17.589	57.42	0.980		23	12.462	71.828	0.956
	30	15.855	33.713	0.963		24	11.034	55.330	0.992
	32	16.066	25.805	0.980		27	7.970	32.279	0.983
	41	13.604	13.585	0.998		29	8.419	21.573	0.993
						37	5.370	5.830	0.918

relationship. Observations from **Figure 5B** showed that the internal friction angle ϕ nearly decreased linearly with the increase of water content. A linear function (**Eq. 3**) was used to represent the relationship between ϕ and water content. Results in **Table 4** implied that this linear equation can well describe the variation of ϕ values with water content, excepting for RC-I samples.

$$c = \alpha e^{\beta w} + \chi \tag{2}$$

$$\phi = aw + b \tag{3}$$

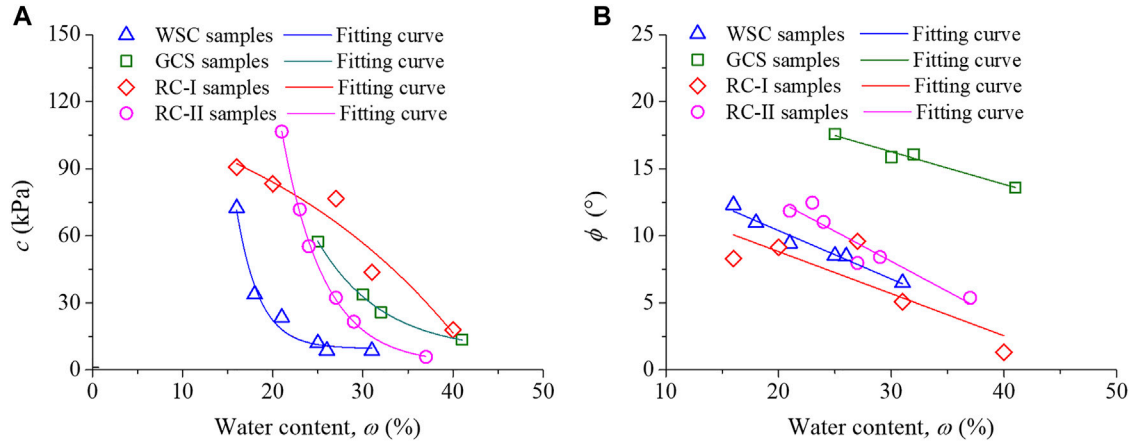

FIGURE 5 | Variations of cohesion c and internal friction angle ϕ with water content for several residual-soil samples.

TABLE 3 | Fitting results for relationship between the cohesion and water content.

Samples	Fitting parameters			R^2
	A	*B*	*X*	
WSC	34945.338	−0.396	9.599	0.972
GCS	1,583.817	−0.139	8.035	0.994
RC-I	-26.089	0.039	140.964	0.888
RC-II	9,309.764	−0.214	2.663	0.998

TABLE 4 | Fitting results for relationship between internal friction angle and water content.

Samples	Fitting parameters		R^2
	A	*B*	
WSC	−0.361	17.619	0.960
GCS	−0.242	23.514	0.951
RC-I	−0.314	15.092	0.625
RC-II	−0.449	21.574	0.866

where α, β, χ, a and b are fitting parameters, respectively; w is water content.

3.2 Mineral Composition and Microstructure of Residual Soils

3.2.1 Mineral Composition Analysis

Figure 6 shows X-ray diffraction results of WSC, GCS and RC-I samples. The mineral contents of soils are summarized in **Table 5**. It can be seen from **Table 5** and **Figure 6** that the white silty clay sample include rich clay minerals, especially pyrophyllite and illite. Similar observations were also found in gray coal soil, corresponding to 36% for pyrophyllite and 27% for illite. Differently, the main mineral compositions of red clay were kaolinite and quartz, as well as low montmorillonite (12%). Moreover, X-ray diffraction spectra implied that the mineral diffraction peaks for WSC and GCS soils were sharp due to a high content of pyrophyllite, while those of RC-I soil were relatively flat.

3.2.2 Microstructural Analysis

The SEM photos of white silty clay, gray coal soil and red clay (RC-I) are illustrated in **Figure 7**. The microstructure of WSC sample was composed of various-sized aggregates (1–30 μm), which were consisted of clay particles. These clay particles exhibited a loose arrangement with identified inter-particle pores and a poor orientation with face-face and face-edge connections, as shown in **Figure 7B**. Meanwhile, these large-size pores (1–10 μm) between clay particles promoted the connection of air or fluid inside soil, thus resulting in a high permeability. Observations from **Figures 7C,D** revealed that the

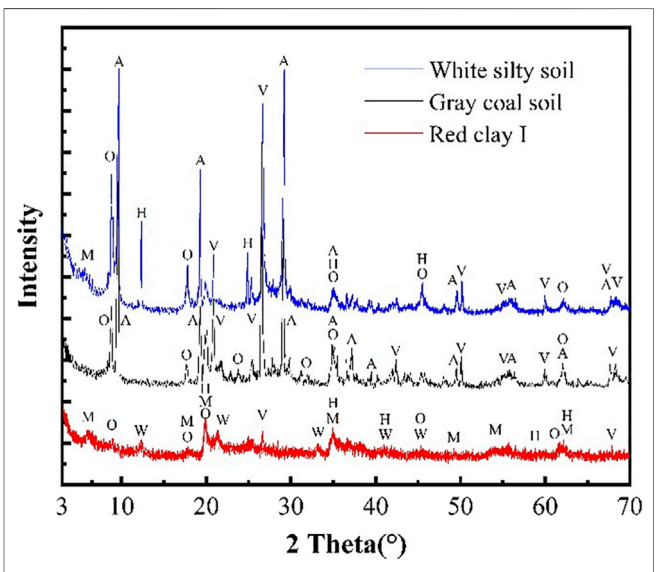

FIGURE 6 | X-ray diffraction spectra of soils in the study area.

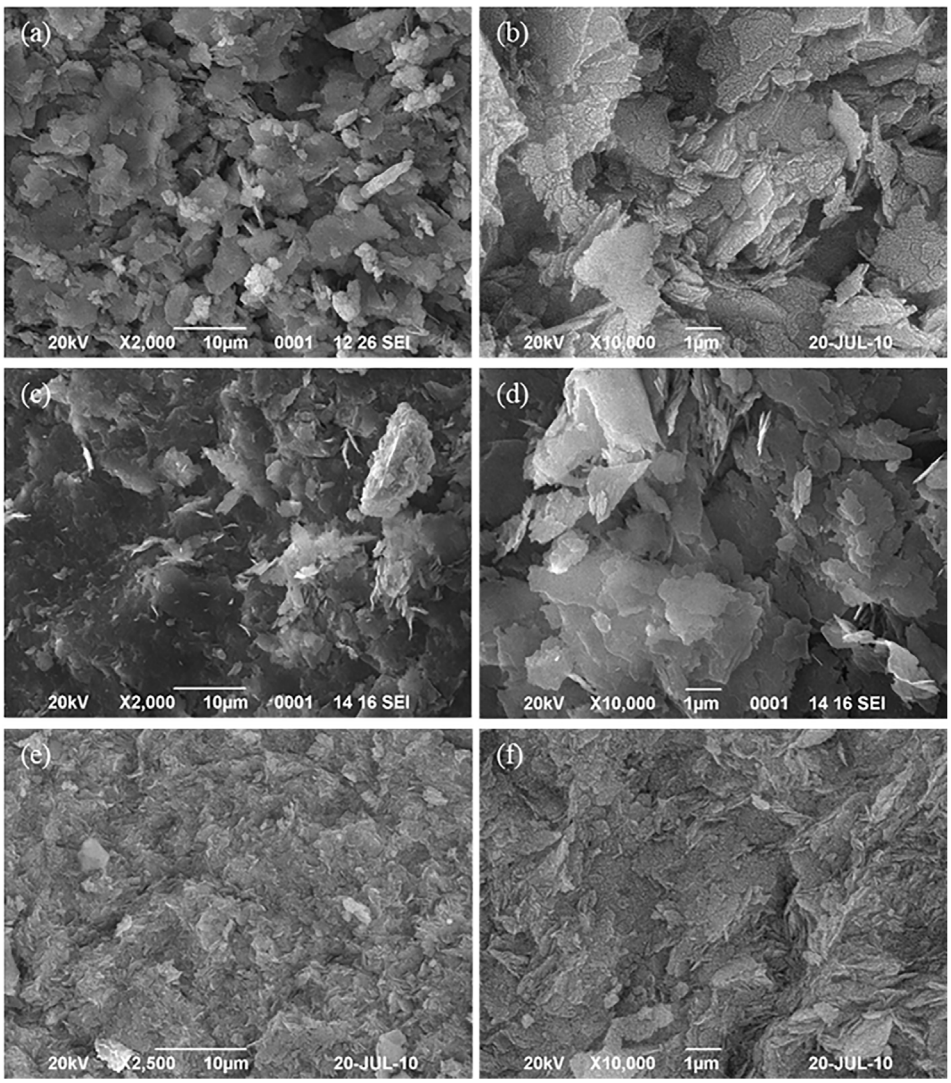

FIGURE 7 | SEM photographs for **(A) (B)** WSC samples; **(C) (D)** GCS samples and **(E) (F)** RC-I samples.

TABLE 5 | Mineral compositions of typical residual soils.

Samples	A	V (%)	O (%)	H	M	W	L	N
WSC	41%	17	20	12%	4%	—	—	Rest
GCS	36%	21	27	—	—	—	—	Rest
RC-I	—	25	7	32%	12%	11%	3%	Rest

A, pyrophyllite; V, quartz; O, illite; H, kaolinite; M, montmorillonite; W, limonite; L, anatase; N, others.

coal-soil structure exhibited a sheet-structure system with an orderly face-face arrangement and a strong orientation between clay particles. Compared with WSC samples, the GCS samples had smaller sized pores and a tighter structure. Thus, the permeability for GCS samples was lower and the anisotropy in mechanical property was more obvious. Similarly, red clay also possessed a face-face structure. The soil particles were arranged in an orderly manner with an obvious orientation. The stratification between particles was discernible, but the boundaries and edges between clay particles could not be clearly identified.

The residual-soil landslide induced by rainfall is substantially due to the reduction in shear strength of the sliding-zone soils. Results in **Figure 3** have demonstrated that the shear strength of soils decreased with increasing water content, indirectly confirming that the rainfall process will cause a decrease in shear strength of slope soils in the field environment. Actually, the reduction of shear strength was actually attributed to microstructural changes inside the soils. Several residual soils studied in this study contained abundant clay minerals, e.g., illite, kaolinite and montmorillonite. During hydration process, these clay minerals would absorb water molecules, generating water films on the surface of clay particles (He et al., 2019; Zhang et al., 2020; He et al., 2022). As the thickness of water films increased,

clay particles separate from each other and the cohesiveness between them gradually reduced. Correspondingly, the clay structure underwent softening and degradation, and the clay minerals transferred from a tightly face-face arrangement to a loosely face-edge or even edge-edge one, leading to a reduction in mechanical strength (Zhang et al., 2016; Lu et al., 2021).

4 CONCLUSION

In this study, the mechanical property of typical residual soils from a landslide zone was investigated by conducting direct shear tests. Meanwhile, mineral composition and microstructures of soil samples were also analyzed through XRD and SEM tests. The obtained results allowed the following conclusions to be drawn:

The shear strength of soils gradually decreased with increasing water content under constant vertical load, but the developing trends of shear strength were influenced by the soil types. At a given water content, the shear strength of all soil samples nearly linearly increased with the increase of vertical loads. The soil cohesion reduced with increasing water content and this change could be well described by an exponential function. Simultaneously, as water content increased, the internal friction angle of soils nearly linearly decreased.

XRD analysis results implied that the main mineral components for white silty clay and gray coal soil were pyrophyllite and illite, corresponding to sharp mineral diffraction peaks. Different from these two samples, red clay had rich kaolinite and montmorillonite and its mineral diffraction peaks were low. SEM observations revealed that white silty clay was consisted of various-sized aggregates. The clay particles inside aggregates exhibited a loose arrangement and a poor orientation. Compared with white silty clay samples, the gray coal soil samples showed an orderly face-face arrangement and a strong orientation between clay particles. In red clay, the soil particles were arranged in an orderly manner, but the boundaries and edges between clay particles could not be clearly identified. The clay minerals inside residual soils absorbed water molecules upon hydration, generating water films on the surface of clay particles. Clay particles separated from each other and gradually transferred from a tightly face-face arrangement to a loosely face-edge or even edge-edge one, resulting in a reduction in the cohesive force between them.

DATA AVAILABILITY STATEMENT

The original contributions presented in the study are included in the article/Supplementary Material, further inquiries can be directed to the corresponding author.

AUTHOR CONTRIBUTIONS

ZZ: Investigation, Writing review and editing YH: Resources, Supervision, Project administration Z-PY: Writing original draft, Methodology BC: Conceptualization, Formal analysis K_NZ: Visualization, Supervision.

FUNDING

The authors thank the National Natural Science Foundation of China (Projects: 42072318 & 41807253) and the Natural Science Foundation of Hunan Province, China (Project 2019JJ50763) for their financial support. The authors also thank the Science and Technology Innovation Program of Hunan Province (Project 2021RC 2004) and the Open Research Fund Program of Key Laboratory of Metallogenic Prediction of Nonferrous Metals and Geological Environment Monitoring (Central South University), Ministry of Education (Project 2021YSJS17).

REFERENCES

Bai, B., Nie, Q., Zhang, Y., Wang, X., and Hu, W. (2021b). Cotransport of Heavy Metals and SiO_2 Particles at Different Temperatures by Seepage. *J. Hydrol.* 597. doi:10.1016/j.jhydrol.2020.125771

Bai, B., Zhou, R., Cai, G. Q., Hu, W., and Yang, G. C. (2021a). Coupled Thermo-Hydro-Mechanical Mechanism in View of the Soil Particle Rearrangement of Granular Thermodynamics. *Comput. Geotech.* 137. doi:10.1016/j.compgeo.2021.104272

De Vita, P., Reichenbach, P., Bathurst, J. C., Borga, M., Crosta, G., Crozier, M., et al. (1998). Rainfall-triggered Landslides: a Reference List. *Environ. Geol.* 35 (2), 219–233. doi:10.1007/s002540050308

Farooq, K., Orense, R., and Towhata, I. (2004). Response of Unsaturated Sandy Soils under Constant Shear Stress Drained Condition. *Soils Found.* 44 (2), 1–13. doi:10.3208/sandf.44.2_1

Fredlund, D. G., Xing, A., Fredlund, M. D., and Barbour, S. L. (1996). The Relationship of the Unsaturated Soil Shear Strength to the Soil-Water Characteristic Curve. *Can. Geotech. J.* 33 (3), 440–448. doi:10.1139/t96-065

He, Y., Hu, G., Wu, D.-Y., Zhu, K.-F., and Zhang, K.-N. (2022). Contaminant Migration and the Retention Behavior of a Laterite–Bentonite Mixture Engineered Barrier in a Landfill. *J. Environ. Manage.* 304, 114338. doi:10.1016/j.jenvman.2021.114338

He, Y., Li, B.-b., Zhang, K.-n., Li, Z., Chen, Y.-g., and Ye, W.-m. (2019). Experimental and Numerical Study on Heavy Metal Contaminant Migration and Retention Behavior of Engineered Barrier in Tailings Pond. *Environ. Pollut.* 252, 1010–1018. doi:10.1016/j.envpol.2019.06.072

He, Y., Wang, M.-m., Wu, D.-y., Zhang, K.-n., Chen, Y.-g., and Ye, W.-m. (2021). Effects of Chemical Solutions on the Hydromechanical Behavior of a Laterite/bentonite Mixture Used as an Engineered Barrier. *Bull. Eng. Geol. Environ.* 80 (2), 1169–1180. doi:10.1007/s10064-020-02003-6

He, Y., Ye, W.-m., Chen, Y.-g., Zhang, K.-n., and Wu, D.-y. (2020). Effects of NaCl Solution on the Swelling and Shrinkage Behavior of Compacted Bentonite under One-Dimensional Conditions. *Bull. Eng. Geol. Environ.* 79 (1), 399–410. doi:10.1007/s10064-019-01568-1

Khan, M. S., Hossain, S., Ahmed, A., and Faysal, M. (2017). Investigation of a Shallow Slope Failure on Expansive Clay in Texas. *Eng. Geol.* 219, 118–129. doi:10.1016/j.enggeo.2016.10.004

Lu, N. (2016). Generalized Soil Water Retention Equation for Adsorption and Capillarity. *J. Geotech. Geoenviron. Eng.* 142 (10), 04016051. doi:10.1061/(asce)gt.1943-5606.0001524

Lu, P.-H., He, Y., Zhang, Z., and Ye, W.-M. (2021). Predicting Chemical Influence on Soil Water Retention Curves With Models Established Based on Pore

Structure Evolution of Compacted Clay. *Comput. Geotech.* 138, 104360. doi:10.1016/j.compgeo.2021.104360

Ma, L.-M., and Tan, Z.-M. (2009). Improving the Behavior of the Cumulus Parameterization for Tropical Cyclone Prediction: Convection Trigger. *Atmos. Res.* 92 (2), 190–211. doi:10.1016/j.atmosres.2008.09.022

Ministry of Housing and Urban-Rural Development of the People's Republic of China (2019). *Standard for Geotechnical Testing Method. GB / T 50123-2019*. Beijing: China Architecture & Building Press.

Miščević, P., and VlastUelica, G. (2014). Impact of Weathering on Slope Stability in Soft Rock Mass. *J. Rock Mech. Geotech.* 6 (3), 240–250. doi:10.1016/j.jrmge.2014.03.006

Mitchell, J. K., and Soga, K. (2005). *Fundamentals of Soil Behavior*. New York: John Wiley & Sons.

Orense, R., Farooq, K., and Towhata, I. (2004). Deformation Behavior of Sandy Slopes during Rainwater Infiltration. *Soils Found.* 44 (2), 15–30. doi:10.3208/sandf.44.2_15

Patuti, I. M., Rifa'i, A., and Suryolelono, K. B. (2017). Mechanism and Characteristics of the Landslides in Bone Bolango Regency, Gorontalo Province, Indonesia. *Int. J. GEOMATE* 12 (29), 1–8. doi:10.21660/2017.29.79901

Sun, Z., Chen, Y.-g., Cui, Y.-j., Ye, W.-m., and Chen, B. (2019). Effect of Synthetic Beishan Site Water and Cement Solutions on the Mineralogy and Microstructure of Compacted Gaomiaozi(GMZ) Bentonite. *Soils Found.* 59 (6), 2056–2069. doi:10.1016/j.sandf.2019.11.006

Wen, M., Chen, A. Q., and Dong, R. (2019). Analysis of the Mechanism of Rain-Induced Slow-Inclination Red Bed Rock Landslide. *Eng. Constr. Des.* 402 (04), 68–70. (In Chinese). doi:10.13616/j.cnki.gcjsysj.2019.02.231

Xiao, T., Yu, L. B., Tian, W. M., Zhou, C., and Wang, L. Q. (2021). Reducing Local Correlations Among Causal Factor Classifications as a Strategy to Improve Landslide Susceptibility Mapping. *Front. Earth Sci.* 9, 997. doi:10.3389/feart.2021.781674

Yin, Y., Wang, L., Huang, B., Zhang, Z., and Dai, Z. (2022). Evolution Analysis of the Banbiyan Dangerous Rock Mass in the Three Gorges Reservoir Area, China. *Georisk Assess. Manag. Risk Eng. Syst. Geohazards* 81 (3), 1–11. doi:10.1080/17499518.2022.2062776

Zhang, C., Li, J. Z., and He, Y. (2021). Impact of the Loading Rate on the Unsaturated Mechanical Behavior of Compacted Red Clay Used as an Engineered Barrier. *Environ. Earth Sci.* 80 (4), 1–12. doi:10.1007/s12665-021-09436-6

Zhang, S., Xu, Q., and Hu, Z. (2016). Effects of Rainwater Softening on Red Mudstone of Deep-Seated Landslide, Southwest China. *Eng. Geol.* 204, 1–13. doi:10.1016/j.enggeo.2016.01.013

Zhang, Z., Ye, W.-M., Liu, Z.-R., Wang, Q., and Cui, Y.-J. (2020). Mechanical Behavior of GMZ Bentonite Pellet Mixtures over a Wide Suction Range. *Eng. Geol.* 264, 105383. doi:10.1016/j.enggeo.2019.105383

Zhu, J. D., Yan, H., Li, S. H., and Wu, L. Z. (2019). Laboratory Model Experiment of Landslides along Loess Mudstone Interface Induced by Rainfall Patterns. *J. Eng. Geo.* 27 (03), 623–631. (In Chinese). doi:10.13544/j.cnki.jeg.2018-139

Conflict of Interest: The authors declare that the research was conducted in the absence of any commercial or financial relationships that could be construed as a potential conflict of interest.

Publisher's Note: All claims expressed in this article are solely those of the authors and do not necessarily represent those of their affiliated organizations, or those of the publisher, the editors and the reviewers. Any product that may be evaluated in this article, or claim that may be made by its manufacturer, is not guaranteed or endorsed by the publisher.

Copyright © 2022 He, Yu, Zhang, Chen and Zhang. This is an open-access article distributed under the terms of the Creative Commons Attribution License (CC BY). The use, distribution or reproduction in other forums is permitted, provided the original author(s) and the copyright owner(s) are credited and that the original publication in this journal is cited, in accordance with accepted academic practice. No use, distribution or reproduction is permitted which does not comply with these terms.